Enhanced conductivity of sodium versus lithium salts. Sodium cobaltacarboranes as electrolytes of choice.

Isabel Fuentes[1], Andreu Andrio[2], Francesc Teixidor[1,*], Clara Viñas[1], Vicente Compañ[3,*].

[1]Institut de Ciència de Materials de Barcelona. Campus UAB, 08193 Bellaterra, Barcelona (Spain)

[2]Departamento de Física aplicada. Universitat Jaume I- 12080, Castellón (Spain)

[3]Escuela Técnica Superior de Ingenieros Industriales. Departamento de Termodinámica Aplicada. Universidad Politécnica de Valencia, Camino de vera s/n, 46020 Valencia, (Spain).

*: Corresponding author:

Abstract

The development of new types of ion conducting materials is one of the most important challenges in the field of the energy. Lithium salts polymer electrolytes have been used as the more usual ion in the design in the new generation of batteries. However in this work we have observed that the incorporation of Na^+ ions provides conductivity superior or at least comparable with this obtained for Li^+ions in the same material-based. This allows foreseeing an excellent possibility to use them in the design of a new generation of batteries, the use of this type of materials with the incorporation of sodium ions to enhance the conductivity. From our results we conclude that the dc-conductivity is larger when the anion is the $[Co(C_2B_9H_{11})_2]^-$, Cosane, against tetraphenylborate, TPB, however the dc-conductivity behavior of Li^+ and Na^+ salts is opposite in the two anions. At 40ºC the conductivity values change from $1.05x10^{-2}$ S/cm (Li-Cosane) and $1.75x10^{-2}$ S/cm (Na-Cosane) to $2.8x10^{-3}$ S/cm (Li-TPB) and $1.5x10^{-3}$ S/cm (Na-TPB). For TPB the dc-conductivity is about one order lower than Cosane, however the dc-conductivity is higher for Na^+ in (Na-Cosane) than in (Li-Cosane) whereas for TPB the conductivity of (Na-TPB) and (Li-TPB) are $2.5x10^{-3}$ S/cm and $6.0x10^{-3}$ S/cm, respectively.

Introduction

Hybrid organic-inorganic composite polymer electrolyte membranes contain inorganic building blocks in the organic polymer. This type of architectures combines properties which require mechanically and thermally stable inorganic backbones with good dielectric and conductivity characteristics. It is desirable that when these inorganic structures are immersed into the organic polymer have good specific chemical reactivity, ductility, flexibility and easy procesability to get membranes for energy applications such as for fuel cells, batteries and supercapacitors.

Due to the varying properties of polymers and inorganic compounds, the selection of materials is key for the preparation of mixed matrix membranes (MMMs) to find systems that optimize the compatibility of the components and their interfacial interactions.

It is generally accepted that the selected inorganic phase should have the following properties: hygroscopic stability, high specific surface area, surface acidity, excellent compatibility with the organic polymeric phase and good conductivity. In this sense many hygroscopic inorganic materials have been investigated to improve the membrane water adsorption and self-humidifying ability to work at moderate and high temperatures. It is known that water entrapped into the metal oxide provide thermal stability and increase the conductivity of the MMMs. For example, Wang et al.[1] and Hara et al.,[2] have observed that by incorporating metal oxides in sulfonated and hydrated MMMs, produces enhancement of the proton conductivity. In this sense, the proton conductivity varies from 10^{-2} S/cm in case of ZrO_2- SO_3H to $5.1x10^{-4}$ S/cm for SnO_2-nH_2O at 30ºC and 100% RH, respectively (RH, relative humidity). On the other hand, the proton conductivity of SnO_2-nH_2O and ZrO_2- nH_2O decreased with a decrease in water vapor pressure at 130-150ºC, although high conductivity can be found even after drying the MMMs at moderate temperatures (up to 120ºC) or with a decrease of % RH. This can be explained because there is an enhancement of the hopping against the vehicular mechanism which is more significant in case of hydrated membranes at low temperatures.[1,2] On the other hand, the incorporation of heteropolyacids (HPA), metal phosphates such as Zirconium phosphate salts and hydrogen salts ($MHXO_4$) is advantageous due to the increase of the porosity between the materials prepared in MMMs.[3-6] For example in hydrogen salts the conductivity at moderate temperatures varies from 10^{-2} S/cm for RbH_2PO_4 (around 140 ºC) until 10^{-4} to $RbHSO_4$ (around 160ºC).[7,8] Further, the characteristics of the central metal is very important for the

performance in conductivity and stability of the composites; for example, the surface acidity, the dimensions and the shape of inorganic particles influences notably the compatibility, the preparation of the composites and their performance in permeability and conductivity.[2,9-13]

In this work we deal on the conductivity moisture and temperature dependence of metallacarboranes. Why on these species? The $[Co(C_2B_9H_{11})_2]^-$ that is represented in Fig. 1, is a sandwich compound that is anionic, with a very low charge density, 1/45, reversibly redox electroactive, highly stable and with many possibilities of derivatization in a stepwise way. This has facilitated that a wide range of E^o values ranging from -1.80 to -0.35 V (vs Fc) are available today just by dehydrohalogenation.[14-16] As ferrocene, $[Co(C_2B_9H_{11})_2]^-$ is an outer sphere electron transfer agent, but contrarily to Fc its range of possible solvents is very wide, from low to high dielectric constants, broadening its possibilities for processability.[17] Further, despite being a purely inorganic molecule it has a substitution behavior comparable or superior to organic frameworks.[18] This is why one would expect for producing hybrid organic/$[Co(C_2B_9H_{11})_2]^-$ materials with innovative features.

Further, just as much as an organic polymer fragment has hydrophobic sites, and depending on the substituents has polar points, $[Co(C_2B_9H_{11})_2]^-$ has hydrophobic characteristics but also polar behavior as has been demonstrated for its ability to produce vesicles, micelles and lamellae.[19-21] These properties, combined with the stepwise halogenations of the metallacarborane that vary the degree of hydrogen and dihydrogen bonding to organic polymer framework, effectively makes these anionic molecules attractive to produce hybrid organic-inorganic composites.

Indeed organic-inorganic hybrid materials between $[Co(C_2B_9H_{11})_2]^-$ and PPy have already been made. In the pyrrole polymerization process a positively charged polymer is produced that is doped with the reversibly redox active $[Co(C_2B_9H_{11})_2]^-$. Indeed the PPy/$[Co(C_2B_9H_{11})_2]^-$ represents an excellent example of the integration at the molecular level, being a genuine example of hybrid materials.[16,22-25]

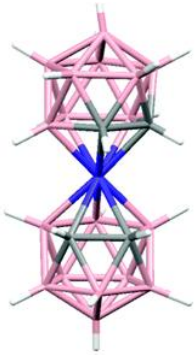

Fig. 1 Molecular representation of $[Co(C_2B_9H_{11})_2]^-$.

These anions display strong non-bonding interactions with themselves and with polymers, inducing properties that are on top of the individual characteristics of the components.

Particularly relevant was the Overoxidation Resistance Limit, ORL, that evidenced an improved resistance to the overoxidation further superior to the one offered by conventional anions.[24] These results and others let to believe that these metallacarboranes can be useful components of MMM and molecular electronics. To this aim we have initiated studies leading to understand their ionic conductivity properties. In this paper we report on the conductivity properties of the more common metallacarborane, the $[Co(C_2B_9H_{11})_2]^-$, and compare the results with the conventional tetraphenylborate $[B(C_6H_5)_4]^-$. Noticeably both $[Co(C_2B_9H_{11})_2]^-$ and $[B(C_6H_5)_4]^-$ have the same charge and the same number of atoms, 45, but have a very different shape, whereas the first is elongated, the second is globular, and binding capacity, whereas the first is able to generate hydrogen and dihydrogen bonding the second is not. This is why the first can self-assemble while the second can't. We are of the opinion that a new class of faradaic electrode materials, these of the metallacarboranes, may emerge as a molecular frontrunner in the field of energy storage systems. Similarly to POMs, metallacarboranes are nanometric clusters with reversible redox activities which can be used as building blocks for energy storage applications.[26]

Experimental

Materials

Lithium tetraphenylborate (Li-TPB), $H[Co(C_2B_9H_{11})_2]$ (H-Cosane), $Na[Co(C_2B_9H_{11})_2]$ (Na-Cosane) and $Li[Co(C_2B_9H_{11})_2]$ (Li-Cosane) were synthesized from commercial samples, $Cs[Co(C_2B_9H_{11})_2]$ (Katchem Spol.sr.o) and Sodium tetraphenylborate (Na-TPB) (Sigma-Aldrich Co). Cationic exchange resin strongly acidic PA was obtained from Panreac.

Synthesis and preparation

The $Na[Co(C_2B_9H_{11})_2]$ was obtained by means of cationic exchange resin from $Cs[Co(C_2B_9H_{11})_2]$. Approximately 2/3 volume of the column (30 cm) was occupied by cationic exchange resin strongly acidic. Before starting, the cationic resin was kept 24 h in HCl 3 M to hydrate it. Then, 150 mL solution of HCl 3M was passed through the column slowly to load it with H^+. To clean the excess of HCl, distilled water was passed

fast till neutral pH. When the desired cation was sodium, a solution of NaCl 3M was passed through the column slowly to change H^+ to Na^+ till neutral pH (the change produce HCl). Distilled water was used to clean the excess of NaCl through the column. To know if NaCl was removed, 3 drops solution of $AgNO_3$ 100 mM was added within a column fraction till see a clear solution. Then, 30 mL of a mix acetonitrile/water (50:50) was passed through the column fast to set up the sample. Approximately 200 mg of the starting compound ($Cs[Co(C_2B_9H_{11})_2]$) was dissolved in a minimum volume of acetonitrile/water (50:50) and passed repeatedly (4 times) through the cationic resin. The sample was collected in a flask, the solvent was finally evaporated and the compound was dried in vacuum.

The $Li[Co(C_2B_9H_{11})_2]$ was obtained by means of cationic exchange resin from $Cs[Co(C_2B_9H_{11})_2]$. The same procedure as $Na[Co(C_2B_9H_{11})_2]$ but instead of loading the column with NaCl 3 M, LiCl 3 M was used. The lithium tetraphenylborate was obtained by means of cationic exchange resin from sodium tetraphenylborate. The same procedure as $Na[Co(C_2B_9H_{11})_2]$ but instead of load the column with NaCl 3 M, LiCl 3 M was used.

The $H[Co(C_2B_9H_{11})_2]$ was obtained by liquid-liquid extraction from $Cs[Co(C_2B_9H_{11})_2]$. Approximately 200 mg of $Cs[Co(C_2B_9H_{11})_2]$ was dissolved in 20 mL diethyl ether. Sample was transferred in a separatory funnel and 15 mL HCl 1 M was added. Two phases were formed and by shaking the sample passed through the organic layer. The organic layer was shaked three times with HCl 1 M (3x 15 mL) to change completely Cs^+ to H^+. The sample was collected in a flask and dried with $MgSO_4$ anhydrous to remove the possible water. Then, the sample was filtered it, the diethyl ether was finally evaporated and the compound was dried in vacuum.

Characterization

The as prepared samples were analyzed by ATR-FTIR, ^1H NMR, $^1H\{^{11}B\}$ NMR, and MALDI-TOF

Characterization of $H[Co(C_2B_9H_{11})_2]$, $Na[Co(C_2B_9H_{11})_2]$ and $Li[Co(C_2B_9H_{11})_2]$. ATR-FTIR (cm-1): 3590, 3561, 3518 (brd, O-H), 3041, 3031 (wk, Cc-H), 2582, 2522 (shp, B-H). MALDI-TOF-MS: m/z calcd for $[Co(C_2B_9H_{11})_2]^-$: 324.76; found: 324.57. ^1H NMR (300 MHz, CD_3OCD_3): δ = 3.97 (br s, 4H, Cc-H). $^1H\{^{11}B\}$ NMR (300 MHz, CD_3OCD_3): δ 3.97 (br s, 4H, Cc-H), 3.41 (s, 2H, B-H), 3.02 (s, 2H, B-H), 2.73 (s, 4H,

B-H), 1.97 (s, 4H, B-H), 1.59 (s, 6H, B-H). ^{11}B NMR (96 MHz, CD_3OCD_3): δ = 7.82 (d, 1J(B,H) = 144 Hz, 2B, B-H), 2.59 (d, 1J(B,H) = 135 Hz, 2B, B-H), -4.15 (m, 8B, B-H), -16.13 (d, 1J(B,H) = 155 Hz, 4B, B-H), -21.64 (d, 1J(B,H) = 167 Hz, 2B, B-H). ^{13}C{1H} NMR (CD_3OCD_3): δ = 50.99 (s, Cc-H).

Samples preparation.

We have measured two types of samples: Cobaltabisdicarbollide, H-, Li-, Na-Cosane and Li-,Na-TPB, each in a dry and in a wet way. Dry ones were prepared by pressing the raw powder into a thin disc 12 mm diameter and about 0.7 mm height. In order to prepare the wet samples, it was first proceeded to regrind the raw material until a very fine powder was obtained. Then, 100 mg of this powder were mixed with 40 mg of ultrapure water thereby obtaining a homogeneous wet paste which retained its appearance throughout the measurement process in a ring of Teflon of 10mm diameter.

Electrochemical impedance spectroscopy (EIS)

The conductivity of the samples in the transversal direction were measured in a range of temperature between 20 and 120°C by impedance spectroscopy in the frequency interval of $10^{-1} < f < 10^{7}$ Hz applying a 0.1 V signal amplitude. The measurements were carried out in dry and wet conditions. A Novocontrol broadband dielectric Spectrometer (BDS) (Hundsangen, Germany) integrated by an SR 830 lock-in amplifier with an Alpha dielectric interface was used. The samples were previously dried and their thicknesses were measured afterwards using a micrometer, taking the average of ten measurements in different parts of the surface. For the study of the conductivity dry conditions the samples were dried in a vacuum cell. Next the samples were sandwiched between two gold circular electrodes coupled to the impedance spectrometer acting as blocking electrodes. The assembly membrane-electrode was annealed in the Novocontrol setup under an inert dry nitrogen atmosphere previously to the start of the actual measurement. For this, firstly a temperature cycle from 20ºC to 120ºC to 20ºC, in steps of 10ºC, was carried out. After this, in a new cycle of temperature scan, the dielectric spectra were collected in each step. This was performed to ensure the measurements' reproducibility and to eliminate the potential interference of water retained by the composite membranes, in particular taking into account the hygroscopicity of this kind of samples. For the measurements in wet conditions the

samples were previously dissolved in bi-distilled water in the ratio 40:60 wt% (sample:water) to obtain a paste which was subsequently sandwiched between the electrodes. During the measurements the electrodes were kept in a BDS 1308 liquid device, coupled to the spectrometer and incorporating deionized water to ensure a fully hydrated state of the samples below 100ºC and in equilibrium with its vapor above 100ºC, to simulate 100% RH atmosphere.[27]

During the conductivity measurements, the temperature was maintained (isothermal experiments) or changed stepwise from 20 to 120ºC controlled by a nitrogen jet (QUATRO from Novocontrol) with a temperature error of 0.1 K during every single sweep in frequency.

From the frequency dependence of complex impedance $Z^*(\omega) = Z'(\omega) + j \cdot Z''(\omega)$, the real part of the conductivity is given as:

$$\sigma'(\omega) = \frac{Z'(\omega) \cdot L}{\left[\left(Z'(\omega)\right)^2 + \left(Z''(\omega)\right)^2 \right] \cdot S} = \frac{L}{R_0 \cdot S} \qquad (1)$$

where L and S are the thickness and area of the sample in contact with the electrodes, respectively.

Results and discussion

Impedance spectroscopy measurements were carried out for all samples at different temperatures to obtain the conductivity. From the complex dielectric measurements, the conductivity was obtained analyzing the data in terms of their dielectric permittivity $\varepsilon^* = \varepsilon' - j\varepsilon''$, where ε' and ε'' represent the real and imaginary parts of the permittivity and j the imaginary unity ($j^2 = -1$). From the imaginary part the conductivity (σ_{dc}) can be calculated when the Maxwell-Wagner-Sillar (MWS)[28-30] effects due to the bulk conductivity dominate as for a pure Ohmic conduction, with $\varepsilon'' = \sigma_{dc}/(\varepsilon_0 \omega)$ where ε_0 represents the permittivity of vacuum and ω the angular frequency of the applied electric field. This can be seen by the fact that the plot of log (ε'') versus log (ω (s^{-1})) yields a straight-line with slope ≈ -1 over an extended range in the region of high frequency. This is the behavior of our samples for all kind of ions incorporated, and for all temperatures studied. From the intersection of this line with log (ω) =0 we can

calculate the dc-conductivity (σ_{dc}). Following this procedure the conductivities of Li-Cosane, Na-Cosane, H-Cosane, Li-TPB and Na-TPB have been obtained in the interval of 20ºC to 120ºC.

Representative spectra of the analyzed samples are shown in Fig. 2. This figure shows the double logarithmic plot of the imaginary permittivity ε" *versus* the frequency for the samples Li-Cosane, Na-Cosane, Li-TPB and Na-TPB, at 50ºC, respectively. For all these samples we have modeled the dielectric loss spectra as a function of the frequency with the piecewise function,[31] by which in the region of moderate frequencies the shoulder has been explained as a Debye relaxation, due to the macroscopic polarization of the ionic charges as consequence of the electric field applied. This relaxation is characterized by a relaxation time τ_{EP}, that depends of sample thickness, temperature and type of polymer.[31-33]

$$\operatorname{Im}\varepsilon'' = \begin{cases} \dfrac{\sigma'}{\varepsilon_0 \omega^n} + \dfrac{\Delta\varepsilon_{EP} \cdot \omega \cdot \tau_{EP}}{1 + (\omega \cdot \tau_{EP})^2} & \text{if} \quad \omega \le \omega_c \\ \dfrac{\sigma_{dc}}{\varepsilon_0 \omega} & \text{for} \quad \omega > \omega_c \end{cases} \tag{2}$$

Where ω_c (=$2\pi f_c$) is a parameter which represents the cut-off frequency that presumably defines the onset of electrode polarization (EP). $\Delta\varepsilon_{EP}$ is the dielectric strength until the EP is fully developed, and the relaxation time τ_{EP} is defined[31] by the bulk resistance R_B and the interfacial capacitance C_{EP} by $\tau_{EP} = R_B \cdot C_{EP}$. The value of τ_{EP} is related to the mean time for an ion crossing from one electrode to another. We interpret the ω_c as the frequency at which the macroscopic electrode polarization is practically irrelevant and, therefore, the changes in the polyelectrolyte to a quasi-ideal conduction can be expressed by the second piece of the function described by equation (2).[31,34] The values of the samples conductivity have been taken as the frequency where the imaginary part of permittivity increases with decreasing frequency as $\varepsilon'' \sim f^{-1}$, exhibiting the typical contribution to the dielectric loss from electrical conduction due to the conductivity of the ionic charges. From this figure we can see that the behavior of Li-Cosane, Na-Cosane, Li-TPB and Na-TPB samples at 50ºC is linear in the region of high frequencies

with a slope practically equal to -1 with a correlation coefficient of 0.999 for all samples and for all the temperatures studied. This is the typical contribution to the dielectric loss from electrical conduction that means that the behavior of the samples for this interval of frequencies is that of a pure conductor.[31] For the sample H-Cosane a similar behavior is observed and it is shown in supplementary section (Fig. S1).

From the intercepts of the straight line observed at the high frequencies region, the value of the dc-conductivity for each temperature has been calculated.

In the region of mid-frequency the behavior of ε" passes through a maximum or a saddle point, then continues increasing with decreasing frequency. This shoulder of the complex permittivity shows a Debye-like shape, due to the electrode polarization (EP) effect, characterized by a relaxation time τ_{EP} that depends on temperature, sample width and chemical structure of materials and its properties. The maximum in ε" represents the full development of the electrode polarization.[35-38] At low frequencies, the dependence is again linear, but with a slope less than unity; this is an indication of a dependence similar to what happens in the high frequency region but with a expression $\varepsilon''=\sigma'/(\varepsilon_0\omega^n)$,[34] in which n takes values between 0.5 to 0.7 but with a conductivity σ' associated to other type of ions such as impurities and some very slow ions, most probably the same cations (Li^+, Na^+, H^+) which are diffusing more slowly because the EP has almost completely build-up.[36]

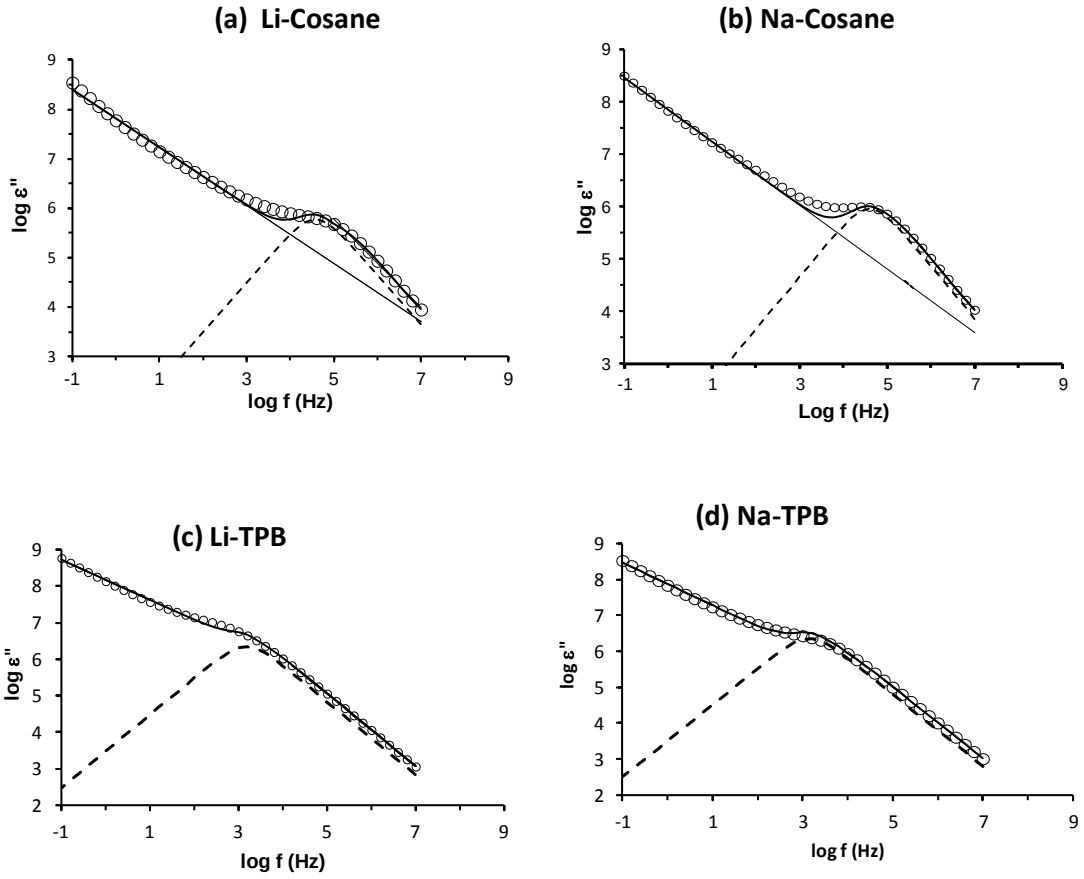

Fig. 2 Dielectric loss spectra as a function of the frequency with the piecewise function for the samples: (a) Li-Cosane, (b) Na-Cosane, (c) Li-TPB and (d) Na-TPB, respectively, at 50ºC. The experimental data of ε"(f) are shown as open circles, the fitted electrode polarization contribution as a dotted line, the solid line represent the fit of equation (2). Also we indicate the fit at low and high frequencies where we obtained the values of σ' and σ_{dc}, respectively, by mean of a line. The exponent *n* for the fit in the low frequencies region for all cases, is between 0.5-0.7 with a correlation coefficient of the adjust r^2= 0.99. The linear fit in the high frequencies region had a slope in between 0.98-1, with r^2=0.999, for all the range of temperatures.

Fig. 3 shows a comparison of the dielectric spectra for all samples at 50ºC. A close inspection of Fig. 3a shows clearly two regions very well differenced. At high frequencies region the real part of the conductivity shows a plateau which starts at frequency, f_c, where the double logarithmic plot of imaginary part of the permittivity versus frequency (Fig. 3c) exhibit a behavior of $\varepsilon'' \sim f^{-1}$ before reaching the maximum characteristic of the full development of electrode polarization (EP). At low frequencies

the dependence is again linear, but with a slope less than unity (n<1) such as indicated above where the dependence of the complex permittivity shows a Debye-like shape, due to electrode polarization effect.

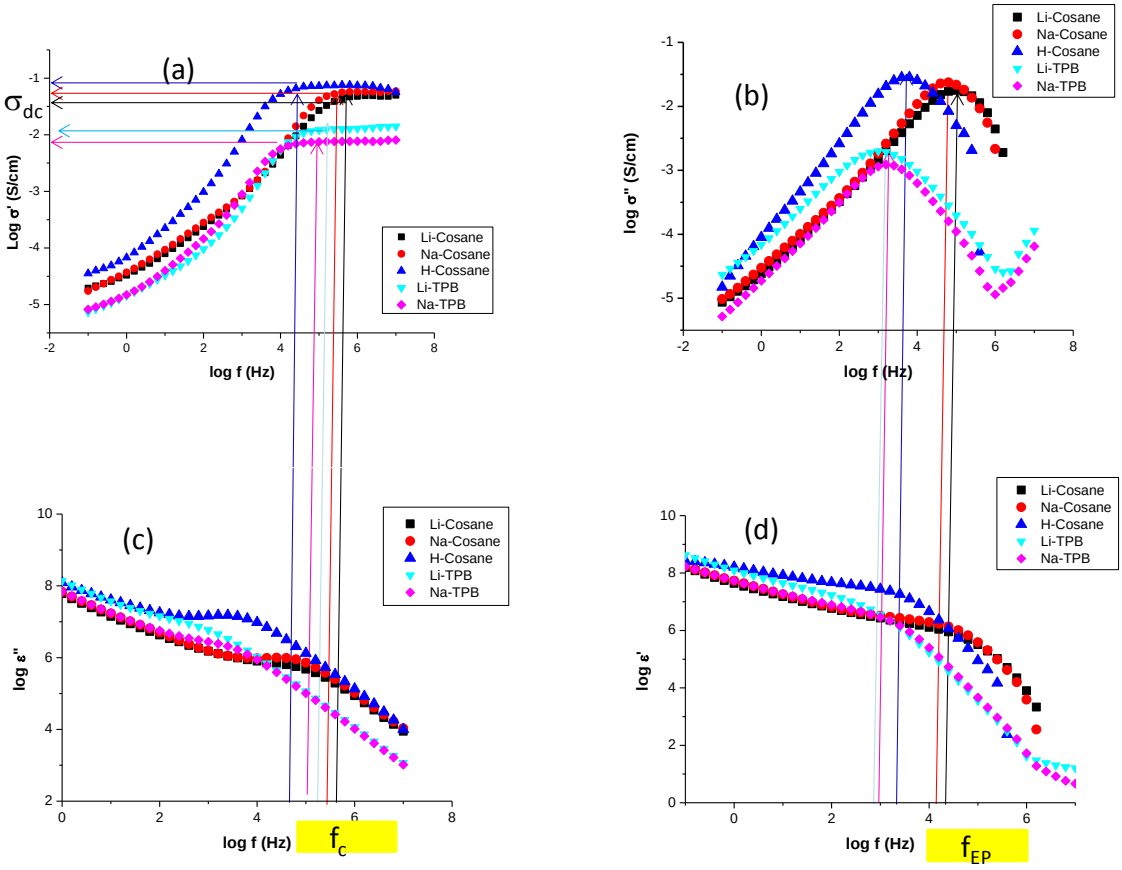

Fig. 3 Double logarithmic plot of real and imaginary parts of the complex dielectric function ε* and real and imaginary parts of the complex conductivity function σ* versus frequency at 50ºC of temperature for Li-Cosane, Na-Cosane, H-Cosane, Li-TPB and Na-TPB, respectively. The arrows in (a) and (c) represent the cut-off frequency (f_c) at which the conductivity has been determined in (a). For this frequency the plot of imaginary part of the permittivity (c) exhibit a behavior of $\varepsilon'' \sim f^{-1}$. In (b) and (d) the arrows determine the frequency at which the full development of the electrode polarization is observed (f_{EP}). At this frequency (f_{EP}), we can see a maximum in (b) and a plateau tendency in (d), which is not get as consequence of the electrode polarization.

Notice that at frequency f_{EP}, where the phase angle reach a value around of 45º in the Bode plot of real part of the conductivity (Fig. 3a), is corresponding with the maximum in the plot of log ε" vs log f (Fig. 3c) and at this frequency the plot of log σ" vs log f (Fig. 3b) reaches a maximum indicative of the full development of the EP where the relaxation time τ_{EP} is determined as $\tau_{EP}=1/(2\pi f_{EP})$. On the other hand in Fig. 3d we can see that the real part of the dielectric permittivity, ε' at f_{EP} turns from the high frequency limit to the static value ε_s. Notice that in the high frequency region (10^6-10^7 Hz) only the sample Li-TPB reach the plateau that correspond to the values of $\varepsilon'(\infty)\cong$ 22. This observed value is slightly higher than those reported as typical for many ionic liquids and glasses[39-41] and also higher than the value found for samples of PPG-LiTFSI(11%).[32] Long distance charge transport across the interfaces produces a distributed MWS relaxation, reflected in the increase of the real part of the permittivity with decreasing the frequency in all the range of temperatures attributed to the electrode polarization (EP). This process may be attributed to the increase deposition of charges at the interfaces of the polymeric materials. However we have not observed the plateau for the other samples. In these systems, structural changes related with the polymer relaxations is controlled by dynamics of the same ions that transport charge, which implies a strong coupling of ion motion to structural dynamics. From the results shown in Fig. 3, we can notice that all samples studied have dielectric spectra similar to the behavior of low molecular weight ionic liquid monomers of 1-vinyl-3-pentyl imidazolium bis(trifluoromethylsulfonyl)imide (PVIM NTf_2).[39] On the other hand, the experimental observation from the dielectric response permit us conclude that for both $\frac{d\varepsilon''}{df}=0$ and $\frac{d\sigma''}{df}=0$ that the peaks observed in the variation of the imaginary part of the conductivity and permittivity appears at the same position in the frequency axe. The conductivity values obtained for all membranes and temperatures are given in Fig. 4.

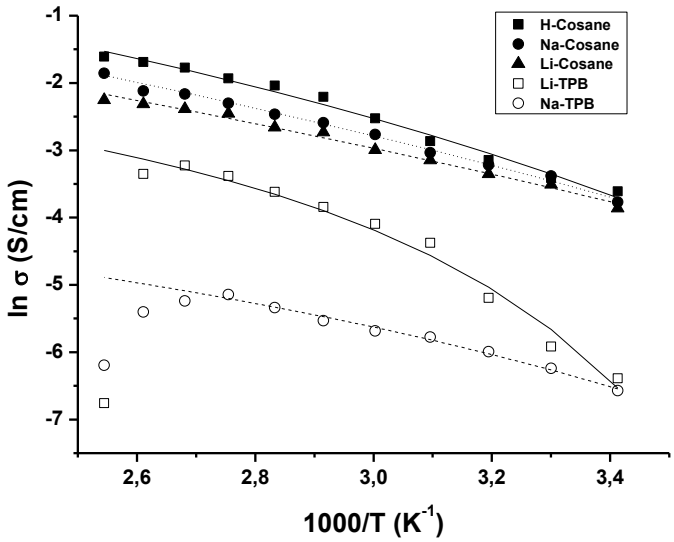

Fig. 4 Conductivity values obtained from the plot of log (ε'') versus log (ω (s^{-1})) in the region of high frequencies where a straight-line with slope ≈ -1 over an extended Bode diagram at frequency where the phase angle was practically zero. The solid line are the fits of experimental data using VFT for I-Cosane (I= Li, Na and H) and I-TPB (I= Li and Na).

From Fig. 4 we observe the temperature dependence of the conductivity values. Most researchers in the field of polymer electrolytes assume that temperature dependence of the conductivity follow approximately a Vogel-Fulcher-Tamman (VFT) equation expressed as:

$$\ln \sigma_{dc} = \ln \sigma_{\infty} - \frac{B}{(T - T_0)} \tag{3}$$

where B is a fitting parameter related with the curvature of the plot that can be seen as the high temperature activation energy of the process underlaying the dc-conductivity, σ_{∞} is the prefactor relkated with the limit conductivity at higher temperatures and T_0 the Vogel temperature, considered as the one at which the relaxation time would diverge. In Table 1 we gathered the corresponding values obtained from the fitting curves shown in Fig. 4.

Table 1 Vogel-Fulcher-Tammann (VFT) parameters obtained from the fit of Fig. 4 for the samples analyzed in this study. The values of χ^2 parameters represent the sum of the square deviations between the experimental data and theoretical values obtained using the equation (3).

Sample	$\ln \sigma_\infty$ (S/cm)	B (K)	T_0 (K)	χ^2	E_{act} (kJ/mol)
H-Cosane	1.38	680±10	160±2	0.06	5.6±0.2
Li-Cosane	0.93	950±10	100±2	0.03	7.9±0.2
Na-Cosane	1.4	940±10	115±2	0.01	7.8±0.1
Li-TPB	-1.2	280±15	240±2	0.02	2.3±0.2
Na-TPB	-2.7	425±10	185±3	0.01	3.5±0.1

In these cases, the mobile ion concentrations are assumed constant with the temperature or follow an Arrhenius behavior. However in most cases the dependence with temperature of mobile ion charges can be more complicated as is happening for PEO^-Li^+, PEO^-Na^+ and PEO^-Cs^+.[31] In our study we can see that all samples can be described following a VFT equation. However, in case of H-Cosane, Li-Cosane and Na-Cosane the tendency linear can be better described with two different slopes, above and below 70-80ºC that differentiate two distinct regions. This is more distinguishable for H-Cosane and less for Li-Cosane, Na-Cosane, although a similar interpretation with two different slopes could be done for Li-Cosane and Na-Cosane.

The conductivity of all samples is strongly humidity dependent increasing more than four or five orders of magnitude in the case of Li-Cosane at 50ºC. For example for the sample Li-Cosane the conductivity at 30ºC is around 10^{-7} S/cm. (Fig. S2). For all temperatures studied the values of the conductivity increase with the temperature following the order σ(H-Cosane) > σ(Na-Cosane) > σ(Li-Cosane).

The calculated activation energy from the VFT and Arrrhenius equations follow the trends E_{ac}(H-Cosane) =5.6 kJ/mol < E_{ac}(Na-Cosane) =7.8 kJ/mol ≅ E_{ac}(Li-Cosane)=7.9 kJ/mol, considering all the interval of temperatures. On the other hand, the activation energy for Li-TPB and Na-TPB are quite similar with values of 2.3 and 3.5 kJ/mol, respectively. However we can observe that in TPB the conductivity of both Na^+ and Li^+ ions decrease near 100-110ºC for Na-TPB and Li-TPB, respectively. For

example the conductivities at 110ºC and 120ºC are $3.5x10^{-2}$ and $1.2x10^{-3}$ S/cm for Li-TPB while for Na-TPB these values are $4.5x10^{-3}$ and $2.0x10^{-3}$ S/cm, respectively.

These E_{ac} values are lower than the corresponding ones obtained for the majority of low molecular weight ionic liquids (ILs)[39] and poly(ethylene oxide)-based sulfonated ionomer[31] with Li^+ and Na^+. These results show that excellent ion mobilities can be obtained with these cobaltacarboranes in wet conditions. The incorporation of Li^+ in place of Na^+ produces a slight increase in activation energy, both being almost identical, when the monomer is Cosane, and are a little higher than with TPB. The values of conductivity are similar to chemical structures containing carboxylic groups and inorganic metallic centre's in their structures at ambient temperature and 100% RH, where the values found are in the range of 10^{-2}-10^{-3} S/cm.[42] However our values are higher than the conductivity obtained in nanocrystalline zeolitic imidazolate framework-8 (ZIF-8) where at 94ºC and 98% RH was around $4.5x10^{-4}$ S/cm.[43] The activation energy values for conduction are smaller in the metallacarborane samples than for ZIF-8 where the values found are surprisingly high, about 110 kJ/mol; more than thirty times these reported here (for Cosane derivatives). Also our results are lower (for the Cosan derivatives) to the values found for several ionic liquids HMIM-BF_4 (molecular weight 254 g/mol), HMIM-Br (molecular weight 247.18 g/mol), HMIM-Cl (molecular weight 202,73 g/mol) and HMIM-I (molecular weight 312.34 g/mol) and more smaller in case of TPB samples, where the values were around 2.9 kJ/mol and ten times lower than these obtained by Rivera and Rossler for different series of imidazolium based ILs.[44,45] As observed in Fig. 4, the dc-conductivity is larger when the monomer is Cosane in place of TPB, however the behavior of Li^+ and Na^+ ions are contrary in each of the monomers. For example, at 40ºC the conductivity values change from $1.05x10^{-2}$ S/cm and $1.75x10^{-2}$ S/cm to $2.8x10^{-3}$ S/cm and $1.5x10^{-3}$ S/cm, respectively, i.e. their change is about one order of magnitude, being these values higher for Na^+ ion in the monomer Cosane whereas the opposite happens for TPB. Both Cosane and TPB are monoanionic and precisely have the same number of atoms, 45. Taking into consideration the important changes in polarity and hygroscopicity associated to the change in the cation from Li^+ to Na^+ or H^+, the presence of retained water could have an influence on the conductivity observed. In this sense the H^+ may be associated as hydronium ion resulting in a greater mobility than Li^+ and Na^+ ions.

In Fig. 5 we plot the electrode polarization time τ_{EP} as a function of the reciprocal of the temperature. As we can see this curve cannot be described through a

simple Arrhenius fit, indicating that in polymeric systems of low molecular weigh a simple dependence with temperature is not generally present.

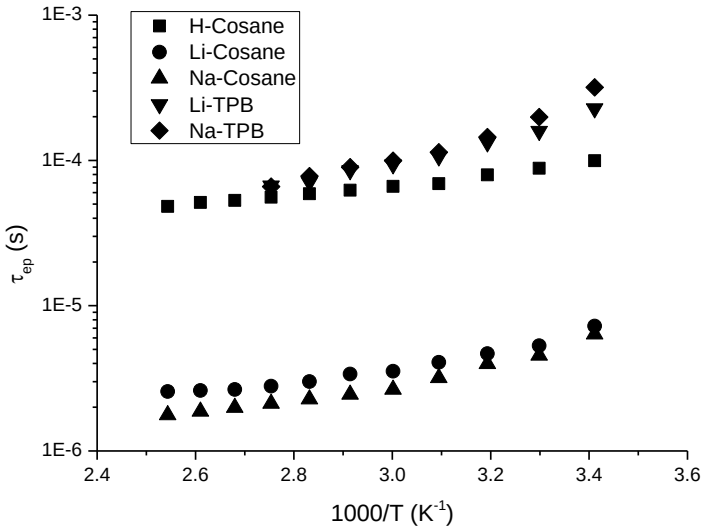

Fig. 5 Temperature dependence of the electrode polarization time τ_{EP}.

Taking in consideration that τ_{EP} represents the mean time for an ion to move from one electrode to another, at times longer than τ_{EP} a large quantity of ions are deposited on the electrodes generating an electric field that retards, therefore, the mobility of like ions. In general, the polarization time of Li^+ and Na^+ ions is at least one order of magnitude smaller than protons in case of monomer Cosane. However this time is larger for TPB than Cosane for both ions. The comparison between Li-Cosane and Na-Cosane suggest that the change in counter cation either Li^+ or Na^+ is not significant in all the range of temperatures, but this relaxation time increases when the cations are protons. This indicates that the counter cations affect the frequency at which the polarization starts to be present in the system. The comparison between the ions in the same monomer Cosane suggests that diffusivity is more effective when the ion is Na^+ and Li^+ than protons. However, a comparison between the monomers suggests that ion transport is more effective in Cosane than TPB for the same ions at the same temperature. It has been demonstrated that charge transport in aprotic ILs is basically characterized by two parameters, namely, the dc-conductivity σ_{dc} and some characteristic diffusion rate ω_c.[44,46,47] Also in our samples we observe that structural relaxation is controlled by dynamics of the same ions that transport charge. This is clear

evidence that a strong coupling of ion motion to structural dynamics exists. However, in our samples the characteristic diffusion rate does not appear because the real part of the conductivity in the high frequencies region finishes in a plateau.

Fig. 6 represents the activation plot for the cut-off frequency f_c for all samples studied. The temperature dependence of the characteristic rates of charge transport for the different cations and monomers show that the activation diffusion rate has an Arrhenius behavior.

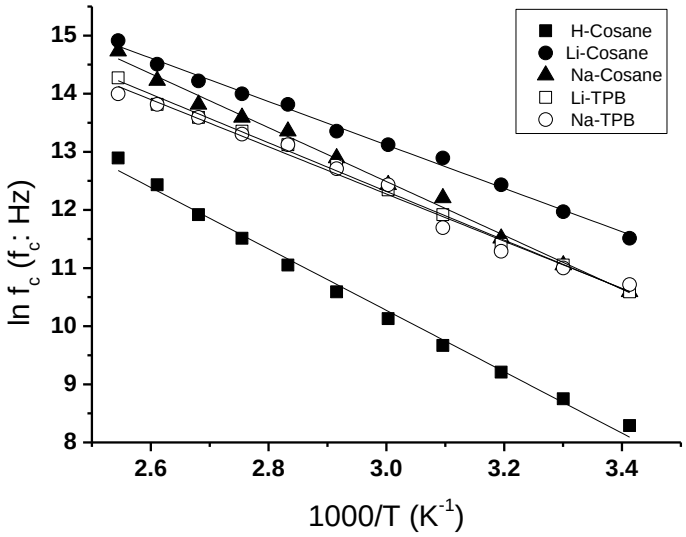

Fig. 6 Activation plot for the characteristic diffusion rate f_c (obtained from plateau of Bode plot of conductivity) for all samples.

The key parameter to describe the charge transport in equation (2) is the cut-off frequency (f_c). This value represents the characteristic frequency at which the real part of the conductivity σ' begins to reach a plateau with decreasing frequency. The comparison between the samples for different type of ions permits to observe that the characteristic frequency of Li-Cosane is slightly larger than Na-Cosane, but in both cases this frequency is about two times the value for H-Cosane. When the monomer change from Cosane to TPB the frequency at the electrode polarization begins to diminish considerably and is slightly lower for Li-TPB than Na-TPB. However at low

temperatures the characteristic frequency for H-Cosane and Na-TPB are practically the same.

The temperature dependence of charge transport is approximately given by Arrhenius behavior as:

$$\ln f_c(T) = \ln f_\infty - \frac{E_{act}}{T} \tag{4}$$

Where f_∞ is the limit cut-off frequency related with the relaxation rate in the high temperature . E_{act} is the activation energy related with the relaxation rate of the process. The activation energy estimate from the Arrhenius equation (4) follow the trend E_{ac}(H-Cosane) = 5.30±0.15 kJ/mol < E_{ac}(Na-Cosane) =4.63±0.11 kJ/mol < E_{ac}(Li-Cosane) =3.73±0.09 kJ/mol, considering all the interval of temperatures. These values are comparables to those obtained for Krause et al.[44] for different Imidazolium-based ionic liquids.

To study the correlation between conduction and dielectric relaxation we proceed to study the validity of the relation proposed by Barton-Nakajima-Namikawa (BNN)[48-50] given by the expression:

$$\sigma_{dc} = B\varepsilon_0 \cdot \Delta\varepsilon \cdot \omega_c \tag{5}$$

Where B is a constant of order unity, ε_0 is the vacuum permittivity, ε_s the static permittivity and ω_c the cut-off angular frequency ($\omega_c=2\pi f_c$). These scaling relations suggest that conduction and dielectric relaxation have their origins in one diffusion process. Fig. 7 shows the double logarithmic plot of the conductivity versus the angular frequency for all the samples studied.

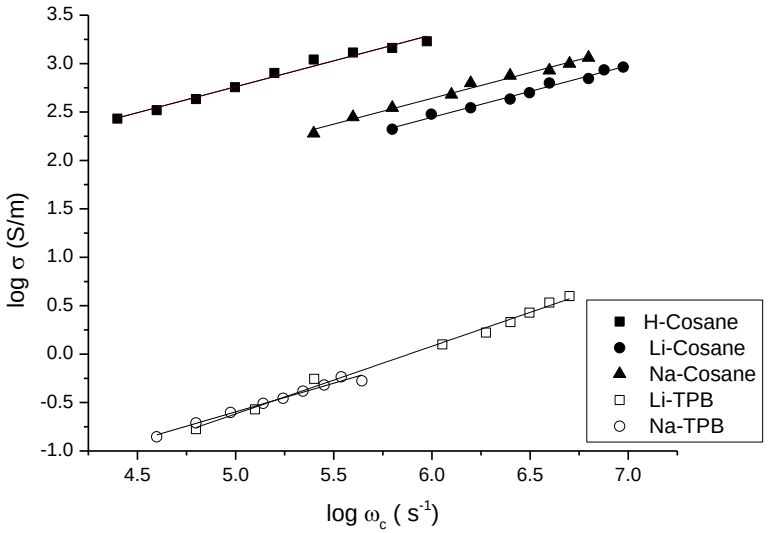

Fig. 7 Double logarithmic plot of the conductivity versus cut-off angular frequency. The solid line corresponds with the fit of BNN relation (equation (3)).

From Fig. 7 we can see the perfect scaling of the conductivity in accordance with equation (5). From these figures we can estimate, considering the value of the parameter B =1, the dielectric strength, $\Delta\varepsilon$. The results obtained are $6x10^7$, $1.5x10^7$, $1.5x10^7$ for the samples H-Cosane, Li-Cosane and Na-Cosane, respectively. While the values of Li-TPB and Na-TPB are approximately around $5x10^6$ in both samples. Further if the static permittivity is known from experimental data the constant B for each sample could be obtained. In our study the static permittivity have not seen possible to determine from experimental values of dielectric spectroscopy impedance and them we can nor give any information about the value of B. Aspects to this question will be discussed in other publication when the metallacarborane $[Co(C_2B_9H_{11})_2]^-$ and some of its halogenated derivatives, together with conventional tetraphenylborate $[B(C_6H_5)_4]^-$ are taking part as a organic-inorganic framework as a mixed matrix membrane (MMMs).

Conclusions

In this work we studied the temperature dependence of ionic conductivity of different ions (Li^+, Na^+ and H^+) incorporated to the more common metallacarborane, the

$[Co(C_2B_9H_{11})_2]^-$, also known as Cosane, and with the conventional tetraphenylborate $[B(C_6H_5)_4]^-$; both with the same number of atoms, with the aim to compare the results.

The possibilities offered by the $M[Co(C_2B_9H_{11})_2]$ (M =Li, Na, H) molecules are very attractive, in particular to produce hybrid organic-inorganic composite membranes of higher conductivity when the hydration is present in its structure.

We have observed that the conductivity of Na^+ ions is superior or at least comparable with the obtained for Li^+ ions in the same material-based. This allows predicting an excellent possibility for their use in the design of a new generation of batteries incorporating sodium ions. Further we have found that the dc-conductivity is larger when the anion is Cosane against TPB, however the dc-conductivity behavior of Li^+ and Na^+ salts is opposite in the two anions. At 40ºC the conductivity values change from $1.05x10^{-2}$ S/cm (Li-Cosane) and $1.75x10^{-2}$ S/cm (Na-Cosane) to $2.8x10^{-3}$ S/cm (Li-TPB) and $1.5x10^{-3}$ S/cm, (Na-TPB). For TPB the dc-conductivity is about one order lower than Cosane, however the dc-conductivity is higher for Na^+ in (Na-Cosane) than Li^+ in (Li-Cosane) whereas for TPB follows (Na-TPB) less than (Li-TPB). In general, the polarization time of Li^+ and Na^+ ions is at least one order of magnitude smaller than protons for Cosane. However the polarization time is larger for TPB than for Cosane both for Li^+ and Na^+. The comparison between Li-Cosane and Na-Cosane suggests that the change in counter cation either Li^+ or Na^+ is not significant in all the range of temperatures, but this relaxation time increases when the cations are protons. This indicates that the counter cations affect the frequency at which the polarization starts to be present in the system. These results derive that the diffusivity of ions in Cosane will be higher than TPB.

The slope of the ε" versus frequency confirmed that ionic mobility at higher frequency region is in concordance with the f_c observed from the Bode diagram for all the samples and temperatures studied. From dielectric response we can conclude that for both $\frac{d\varepsilon''}{df}=0$ and $\frac{d\sigma''}{df}=0$ the peaks or shoulder observed in the variation of the imaginary part of the conductivity and permittivity, respectively, appears at the same position in the frequency axe.

Finally it is important to note that metallacarboranes can be useful components of MMMs providing excellent conductivity when the medium contain sufficient amount of ionic component and certain degree of humidity.

Acknowledgements

This research has been supported by the ENE/2015-69203-R project, granted by the Ministerio de Economía y Competitividad (MINECO), Spain.

References

1. C. Wang, E. Chalkova, C. D. Lute, M. V. Fedkin, S. Komarneni, T. C. M. Chung and S. N. Lvov, *J. Electrochem. Soc*, 2010, **157**, B1634-B1642.

2. S. Hara, H. Sakamoto, M. Miyayama and T. Kudo, *Solid State Ionics*, 2002, **154-155**, 679-685.

3. Q. Yang, M. P. Kapoor and S. J. Inagaki, *Am. Chem. Soc.*, 2002, **124**, 9694-9695.

4. D. Margolese and J. Melero, *J. Chem. Mater*, 2000, **12**, 2448-2459.

5. Y. G. Yin, S. Z. Qiao, Z. P, Xu, J. C. Diniz da Costa and G. Q. Lu, *J. Phys Chem C*, 2009, **113**, 3157-3163.

6. S. Fujita, A. Koiwai, M. Kawasumi and S. Inagaki, *Chem .Mater*, 2013, **25**, 1584-1591.

7. V. G. Ponomareva, B. V. Merinov and V. V. Dolbinina, *Solid State Ionics*, 2001, **145**, 197-204.

8. M. Vijayakumer, A. D. Bain and G. R. Goward, *J. Phys. Chem C*, 2009, **113**, 17950-17957.

9. S. Hara, S. Takano and M. Miyayama, *J. Phys. Chem. B*, **108**, 5634-5639.

10. Y. Kozawa, S. Suzuki, M. Miyayama and T. Okumiya, *Solid State Ionics*, 2010, **181**, 348-353.

11. R. R. Abbaraju, N. Dasgupta and A. V. Virkar, *J. Electrochem. Soc.*, 2008, **155**, B1307-B1313.

12. E. Chalkova, M. V. Fedkin, D. J, Wesolowski and S. N. Lvov, *J. Electrochem. Soc.*, 2005, **152**, A1742-A1747.

13. A. Sahu, G. Selvarani, S. Pitchumani, P. Sridhar and A. Shukla, *J. Electrochem. Soc.*, 2007, **154**, B123-B132.

14. P. González-Cardoso, A. Stoica, P. Farràs, A. Pepiol, C. Viñas and F. Teixidor, *Chem. Eur. J*., 2010, **16**, 6660-6665.

15. A. Pepiol, F. Teixidor, R. Sillanpää, M. Lupu and C. Viñas, *Angew. Chem. Int. Ed*., 2011, **50**, 12491-12495.

16. M. Tarrés, V. S. Arderiu, A. Zaulet, C. Viñas, F. F. de Biani and F. Teixidor, *Dalton Trans*, 2015, **44**, 11690-11695.

17. F. Teixidor, C. Viñas, A. Demonceau and R. Núñez, *Pure Appl. Chem*., 2003, **75**, 1305-1313.

18. D. Olid, R. Nuñez, C. Viñas and F. Teixidor, *Chem. Soc. Rev*. 2013, **42**, 3318-3336.

19. P. Bauduin, S. Prevost, P. Farràs, F. Teixidor, O. diat and T. Zemb, *Angew. Chem. Int. Ed*., 2011, **50**, 5298-5300.

20. D. Brusselle, P. Bauduin, L. Girard, A. Zaulet, C. Vinas, F. Teixidor, I. Ly and O. Diat, *Angew. Chem. Int. Ed*., 2013, **52**, 12114-12118.

21. P. M. Gassin, L. Girard, G. Martin-Gassin, D. Brusselle, A. Jonchere, O. Diat, C. Viñas, F. Teixidor and P. Bauduin, *Langmuir*, 2015, **31**, 2297-2303.

22. C. Masalles, S. Borrós, C. Viñas and F. Teixidor, *Adv. Mater*., 2000, **12**, 1199-1202.

23. C. Masalles, S. Borrós, C. Viñas and F. Teixidor, *Adv. Mater*., 2002, **14**, 449-452.

24. C. Masalles, F. Teixidor, S. Borrós and C. Viñas, *J. Organomet. Chem*., 2002, **657**, 239-246.

25. C. Masalles, J. Llop, C. Viñas and F. Teixidor, *Adv. Mater*., 2002, **14**, 826-829.

26. J. Suarez-Guevara, V. Ruiz and P. Gomez-Romero, *Phys. Chem. Chem. Phys*., 2014, **16**, 20411-20414.

27. F. J. Fernández-Carretero, V. Compañ and E. Riande. *J. Power Sources*, 2007, **173**, 68–76.

28. J. C. Maxwell, *A treatise of Electricity & Magnetism*, Dover N.Y, 1954.

29. K.W. Wagner, *Arch. Elektrotech*, 1914, **2**, 371-387.

30. [a]K.W. Wagner, *Arch. Elektrotech*, 1914, **3**, 67-106; [b]R. W. Sillars, *Proc. Inst. Electr. Eng. London*, 1937, **80**, 378-394.

31. J. Klein, S. Zhang, S. Dou, B. H. Jones, R. Colby and J. Runt, *J. Chem Phys*., 2006, **124**, 144903, 1-8.

32. R. Coelho, *Revue Phys. Appl.*, 1983, **18**, 137-146.

33. J. R. MacDonald, *Phys Rev.*, 1953, **92**, 4-17.

34. A. Munar, A. Andrio, R. Iserte and V. Compañ, *J. Non-Cryst. Solids*, 2011, **357**, 3064-3069.

35. Y. W. Che-Nan, F. Fan, J. R. Sangoro, M. B. Berman, S. G. Greenbaum, T. A. Zawodzinski and A. P. Sokolov, *Phys. Rev. E*, 2013, **87**, 04230l-042308.

36. T. S. Sorensen, V. Compañ, R. Diaz-Calleja and E- Riande, *J Appl. Phys.*, 1996, **79**, 403-411.

37. Y. W. Che-Nan, F. Fan, J. R. Sangoro, M. B. Berman, S. G. Grenbaum, T. A. Zawodzinski and A. P. Sokolov, *Phys. Rev. E*, 2013, **87**, 042308, 1-9.

38. Y. Wang, F. Fan, A. L. Agapov, T. Sait, J. Yang, X. Yu, K. Hong, J. Mays and A. P. Sokolov, *Polymer*, 2014, **55**, 4067-4076.

39. J. R. Sangoro, C. Iacob, A. L. Agapov, Y. Wanf, S. Berdzinski, H. Rexhausen, V. Strehmet, C. Friedrich, A. P. Sokolov and F. Kremer, *Soft Matter*, 2014, **10**, 3536-3540.

40. H. Wiengärtner, *J. Mol. Liquids*, 2014, **192**, 185-190.

41. M. M. Huang, Y. Jiang, P. Sasisanker, G. W. Driver and H. H. Wiengärtne, *J. Chem. Eng. Data*, 2011, **56**, 1494-1499.

42. M. Sadakiyo, T. Yamada and H. Kitagawa, *J. Am. Chem. Soc.*, 2009, **131**, 9906-9907.

43. P. Barbosa, N. C. Rosero-Navarro, S. Fa-Nian and F. M. L. Figuereido, *Electrochim. Acta*, 2015, **153**, 19-27.

44. C. Krause, J. R. Sangoro, C. C. Iacob and F. Kremer, *J. Phys. Chem B*, 2010, **114**, 382-386.

45. A. Rivera and E. A. Rossler, *Phys. Rev B*, 2006, **73**, 212201, 1-4.

46. J. R. Sangoro, M. Mierzwa, C. Iacob, M Pluch and F. Kremer, *RSC Adv*, 2012, **12**, 5047-5050.

47. J. R. Sangoro and F. Kremer, *Acc Chem Res*, 2012, **45**, 525-532.

48. H. J. Namikawa, *J. Non-Cryst. Solids*, 1974, **14**, 88-100.

49. H. J. Namikawa, *J. Non-Cryst. Solids*, 1975, **18**, 173-195.

50. J. R. MacDonald, *J. Appl. Phys.*, 2010, **107**, 101101, 1-9.

51. U. H. Choi, A. Mittal, T. L. Price, H. W. Gibson, J. Runt and R. H. Colby, *Macromolecules*, 2013, **46**, 1175-1186.